RSC Advances

PAPER

View Article Online
View Journal | View Issue

Cite this: *RSC Adv.*, 2017, **7**, 56289

Highly sensitive and selective fluorescence detection of Hg^{2+} based on turn-on aptamer DNA silver nanoclusters†

Baozhu Zhang[ab] and Chunying Wei *[a]

Received 19th October 2017
Accepted 5th December 2017

DOI: 10.1039/c7ra11566k

rsc.li/rsc-advances

A novel turn-on Hg^{2+} sensor was constructed based on fluorescent C–Hg^{2+}-aptamer DNA-stabilized Ag nanoclusters (DNA–AgNCs), and was used to determine the concentration of Hg^{2+} over the range 2–18 nM with a detection limit as low as 0.25 nM. The sensing assay relied on a target-induced conformational transition of Hg^{2+}-aptamer DNA. The conformational change of Hg^{2+}-aptamer DNA from a single strand to a hairpin DNA due to the formation of a T–Hg^{2+}–T complex in the presence of Hg^{2+} made the two darkish DNA–AgNCs approach each other closely and then enhanced the fluorescence of the AgNCs, which enabled the sensitive and specific detection of Hg^{2+}. The proposed sensor was found to be easy to use, and allowed for the sensitive, selective, and turn-on detection of Hg^{2+}. Furthermore, this approach has also been successfully applied to the detection of Hg^{2+} in real water samples, so this sensor may find application in monitoring Hg^{2+} in environmental samples.

1 Introduction

Hg^{2+} is a highly toxic metal ion, and causes, even at low concentrations, severe damage to various organs such as the brain and kidneys and to the nervous, endocrine and cardiovascular systems.[1–3] Therefore, many methods have been developed for detecting Hg^{2+} in recent years, including electrochemical methods,[4,5] atomic absorption/emission spectroscopy,[6,7] fluorescence resonance energy transfer,[8] use of electrochemiluminescence sensors,[9] inductively coupled plasma mass spectrometry,[10,11] high-performance liquid chromatography,[12] and atomic fluorescence spectroscopy.[13] However, these methods have disadvantages, in particular they either require special instrumentation or take a lot of time to perform. Alternatively, molecular fluorescence-based methods have garnered special attention owing to their high sensitivity, good selectivity, and low-cost instruments, particularly in those systems involving DNA,[14] small molecules,[15] peptides, and proteins.[16,17]

Fluorescent noble metal nanoclusters, including gold/silver nanoclusters comprising a few to tens of atoms, have attracted great interest due to their good photostability, low toxicity, excellent biocompatibility, and ultrasmall size. They have been applied as fluorescent probes and photoluminescent and electroluminescent materials for bio-labeling, bio-imaging, and ultrasensitive biological detection.[18,19] Noble metal nanoclusters are often synthesized by employing templates such as amino acids, thiols, proteins, dendrimers, and DNA.[20–24] Among them, the fluorescent Ag nanoclusters using DNA as the scaffold (DNA–AgNCs) have attracted special attention[25,26] because of their outstanding spectral and photophysical properties and tunable fluorescence properties from blue to near-infrared emission that is realized by varying the base sequences or strand lengths of the oligonucleotides.[27,28] Ag^{+} ions bind selectively to the heterocyclic bases of the DNA oligonucleotides rather than to their phosphate and sugar groups.[29] In particular, Ag^{+} can selectively coordinate with the cytosine base.[30] Ag atoms reduced by $NaBH_4$ bind very tightly to cytosines of oligonucleotide, rendering them chemically stable in biological buffers. Fluorescent metal nanoclusters have been employed for the detection of Hg^{2+},[31,32] but most of them are 'light-off' sensors,[28,31,32] which are undesirable from the sensing point of view due to susceptibility to false signals, large background variation, and the limited room for signal change. To overcome these problems, some 'light-up' sensors to detect Hg^{2+} have been designed.[14,33] However, it is very challenging to develop low-cost, easy-to-use, highly sensitive, real-time turn-on sensors of Hg^{2+} based on metal nanoclusters.

Inspired by the fluorescence light-up phenomenon resulting from placing two darkish DNA–AgNCs together to form a probe pair through their complementary linkers,[34] we herein used a similar procedure to construct a novel Hg^{2+} sensor, and the working principle of the proposed assay is depicted in Scheme 1. The DNA template included two segments, one was a thymine

[a]*Key Laboratory of Chemical Biology and Molecular Engineering of Ministry of Education, Institute of Molecular Science, Shanxi University, Taiyuan 030006, P. R. China. E-mail: weichuny@sxu.edu.cn*

[b]*College of Chemistry and Chemical Engineering, Jinzhong University, Yuci 030600, P. R. China*

† Electronic supplementary information (ESI) available. See DOI: 10.1039/c7ra11566k

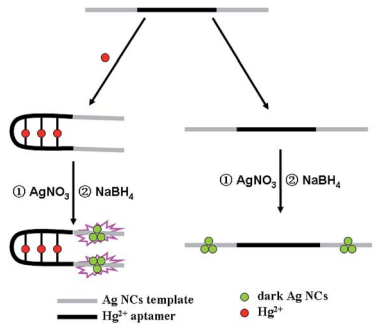

Scheme 1 Schematic illustration of the strategy used to detect Hg^{2+}. This strategy is based on ssDNA-templated silver nanoclusters combining with an Hg^{2+} aptamer.

(T)-containing Hg^{2+} aptamer segment (Hg^{2+}-aptamer-1 and Hg^{2+}-aptamer-2, Table S1†) in the middle of the DNA template, and the other was AgNC-nucleation segments at the two termini. Hg^{2+} has been shown to specifically bind to two thymine (T) residues of DNA to form the T–Hg^{2+}–T complex.[35] Therefore, the hairpin structure formed by C–Hg^{2+}-aptamer-AgNCs (Table S1†) in the presence of Hg^{2+} made the two darkish DNA–AgNCs approach each other closely and then enhanced the fluorescence of the DNA–AgNCs, which enabled the sensitive and specific detection of Hg^{2+}. This approach provided for a novel fluorescent turn-on chemical assay avoiding the need to design a complicated fluorescent sensor and use an organic solvent.

2 Experimental

2.1 Reagents and apparatus

The DNA oligonucleotides used in this work were obtained from Sangon Biotechnology Inc. (Shanghai, China). The sequences of these oligonucleotides are listed in Table S1.† $NaBH_4$, $AgNO_3$, $NaNO_3$, KNO_3, $Mg(NO_3)_2$, $CaCl_2$, $Cu(NO_3)_2$, $Zn(NO_3)_2$, $Cd(NO_3)_2$, $Hg(NO_3)_2$, $Fe(NO_3)_3$, $Co(NO_3)_2$, $Pb(NO_3)_2$, $Mn(NO_3)_2$, $Cr(NO_3)_3$, and $TbCl_3$ were provided by Aladdin Bio-Chem Technology Co. Ltd. (Shanghai, China). All chemical reagents were of analytical grade and used as received without further purification. Phosphate buffer solution (PBS, 20 mM, pH 6.6 or 6.3) was used in all of the experiments. All solutions were prepared using Milli-Q water.

Fluorescence spectra were acquired on a Fluoromax-4 spectrofluorometer (Horiba Jobin Yvon Inc., France), and the slit widths were 10 nm and 5.0 nm for emission and excitation, respectively. UV-Vis absorption measurements were recorded on a Cary 50 Bio spectrophotometer (Varian Inc., CA). Time-resolved fluorescence measurements were taken using an FL920 fluorescence lifetime spectrometer (Edinburgh Instruments, Livingston, UK) operating in the time-correlated single photon counting (TCSPC) mode. For data analyses, commercial software by Edinburgh Instruments was used. The average excited-state lifetime was expressed by using the equation $\tau_{avg} = \sum_{i=1}^{n} A_i\tau_i$, when $\sum_{i=1}^{n} A_i = 1$. The reported spectrum of each sample represented the average of three scans. The average sizes and morphologies of the DNA–AgNCs were characterized by using a JEOL JEM-2100 transmission electron microscope with an acceleration voltage of 200 kV. CD spectra were acquired by using a Chirascan circular dichroism spectrometer (Applied Photophysics Ltd., Surrey, UK), and the spectrum was recorded from 220 to 320 nm at 1 nm intervals using a quartz cell with a 1 mm optical path length and an instrument scanning speed of 120 nm min^{-1} at room temperature. X-ray photoelectron spectroscopy (XPS) (ESCAL-ab 220i-XL, VG Scientific, England) was performed by using monochromic Al K-alpha radiation as a source at 1486.6 eV.

2.2 Preparation of DNA–AgNCs and fluorescence assay of Hg^{2+}

DNA–AgNCs were synthesized according to our previously reported method but with minor modifications.[36] Briefly, the DNA oligonucleotides (0.3 nM) were mixed with various concentrations (0–30 nM) of Hg^{2+} ions in PBS buffer (20 mM, pH 6.6 for C–Hg^{2+}-aptamer-1-AgNCs, and pH 6.3 for C–Hg^{2+}-aptamer-2-AgNCs) and then incubated for 10 min. Then, an $AgNO_3$ aqueous solution was added to the mixture under vigorous shaking for 30 s, and the resulting mixture was kept in the dark at 4 °C for 20 min, followed by being reduced with freshly prepared $NaBH_4$ with vortexing for 1 min. The final concentrations of DNA, $AgNO_3$, and $NaBH_4$ were 0.3, 1.8, and 1.8 μM, respectively. The final C–Hg^{2+}-aptamer-1-AgNC and Hg^{2+}-aptamer-2-AgNC mixtures were stored in the dark at 4 °C for 2.5 hours and one hour, respectively, and these incubation times were calculated based on the amount of $NaBH_4$ added. The fluorescence spectrum of each sample was monitored at room temperature.

2.3 Selective detection of Hg^{2+}

The selectivity of the fluorescence assay was measured by testing 13 different metal ions, specifically Na^+, K^+, Mg^{2+}, Ca^{2+}, Cu^{2+}, Zn^{2+}, Cd^{2+}, Fe^{3+}, Co^{2+}, Pb^{2+}, Mn^{2+}, Cr^{3+}, and Tb^{3+}. The concentrations of Hg^{2+} and the other metal ions were 0.01 and 0.1 μM, respectively. The assay method used for the other metal ions was same as that used for Hg^{2+}.

2.4 Circular dichroism measurements

A concentration of 5.0 μM of each C–Hg^{2+}-aptamer was first mixed with or without 20 nM Hg^{2+} in 20 mM PBS buffer (pH 6.6 or 6.3), and then C–Hg^{2+}-aptamer-DNA–AgNCs were prepared according to the method described above (see Section 2.2). Subsequently, CD spectra of the DNA–AgNCs were acquired.

2.5 Analytical applications

To evaluate the practical application of the probe for the detection of Hg^{2+} in real samples such as tap water and lake water (from Shanxi University), the samples were spiked with standard Hg^{2+} solutions of various known concentrations, and the actual samples were measured under the same condition as that in the buffer.

3 Results and discussion

3.1 Characterization of the DNA–AgNCs

Two different DNA sequences, C–Hg^{2+}-aptamer-1 and C–Hg^{2+}-aptamer-2 (Table S1†), were designed as the templates to form the DNA–AgNCs, in which the Hg^{2+} aptamer segment was in the middle of the template (italic), while the C-rich segments were at the 5′ and 3′ ends, respectively (bold). The optical characterizations of C–Hg^{2+}-aptamer-1-AgNCs in the absence and presence of 10 nM Hg^{2+} are shown in Fig. 1A. Both UV-Vis absorption spectra of C–Hg^{2+}-aptamer-1-AgNCs alone (curve a) and with 10 nM Hg^{2+} (curve b) showed two peaks at wavelengths of 430 and 560 nm, and the peak at 430 nm was the characteristic plasmon absorption band of the Ag nanoparticles[37,38] and the peak at 560 nm was likely the AgNC absorption band. Fig. S1A and B† show the fluorescent emission spectra of C–Hg^{2+}-aptamer-1-AgNCs in the absence and presence of 10 nM Hg^{2+} under various excitation wavelengths, respectively, and the DNA–AgNCs displayed excitation wavelength-dependent emission properties. Upon excitation at 560 nm, the C–Hg^{2+}-aptamer-1-AgNCs in the absence and presence of Hg^{2+} presented a maximum emission peak at 620 nm, but the fluorescence intensity of the latter was about nine times stronger than that of the former (Fig. 1B); this difference may have been due to the Hg^{2+}-aptamer-1 DNA being folded into a hairpin-shaped structure in the presence of Hg^{2+} and hence making the two darkish DNA–AgNCs approach each other closely, resulting in the relatively strong fluorescence (Scheme 1). To confirm this

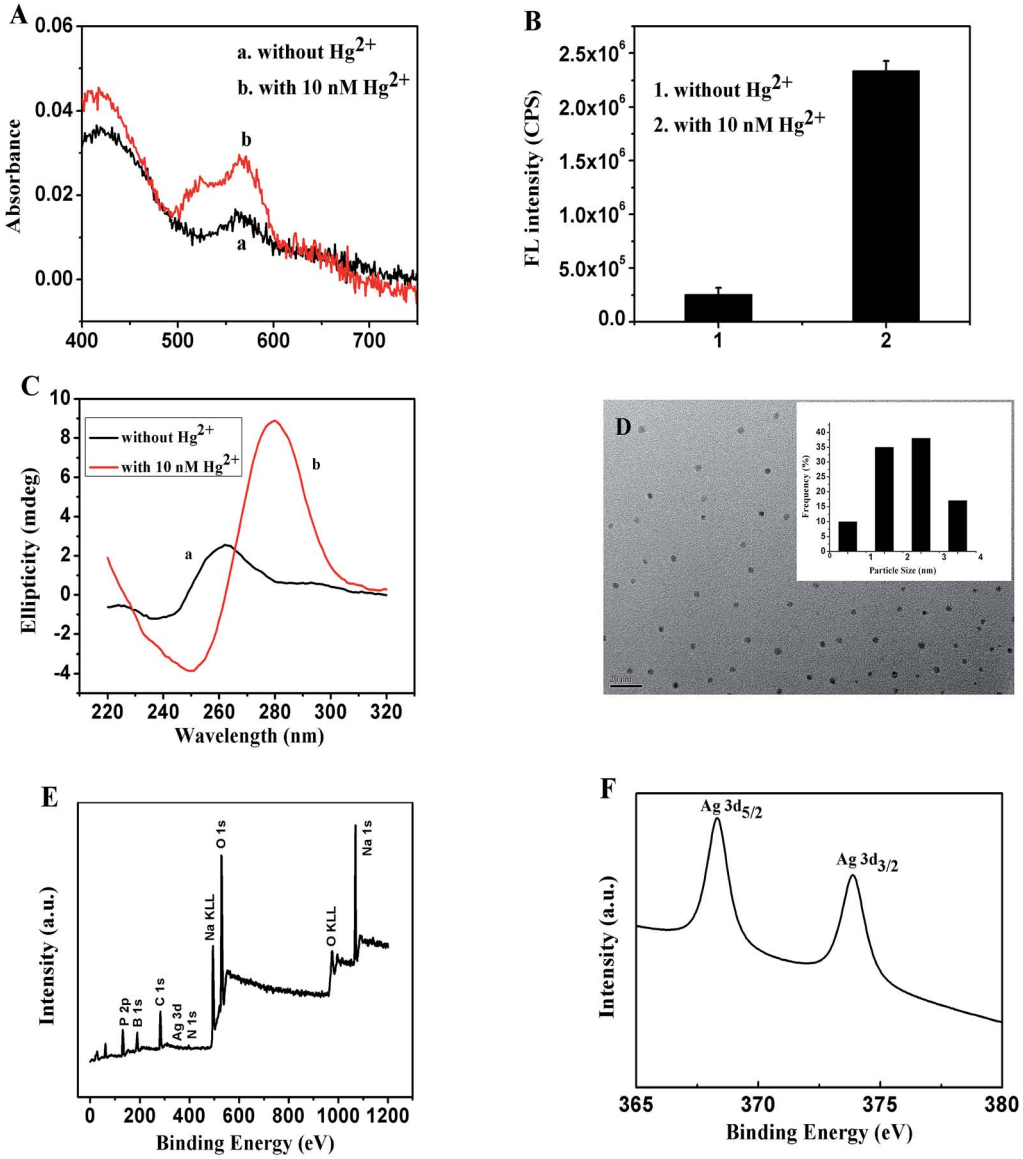

Fig. 1 (A) UV-Vis spectra of C–Hg^{2+}-aptamer-1-AgNCs in the absence (a) and presence of 10 nM Hg^{2+} (b). (B) The fluorescence intensities of C–Hg^{2+}-aptamer-1-AgNCs in the absence (1) and presence of 10 nM Hg^{2+} (2). (C) CD spectra of C–Hg^{2+}-aptamer-1-Ag NCs without (a) and with 20 nM Hg^{2+} (b) in 20 mM PBS buffer (pH 6.6). (D) TEM image of C–Hg^{2+}-aptamer-1-AgNCs in the presence of 10 nM Hg^{2+}. The inset shows the size distribution histogram. (E) XPS spectrum of C–Hg^{2+}-aptamer-1-AgNCs. (F) Ag 3d region of the XPS spectrum of C–Hg^{2+}-aptamer-1-AgNCs. All measurements were taken in 20 mM PBS buffer (pH 6.6).

proposal, CD spectra of the C–Hg^{2+}-aptamer-1-AgNCs in the absence and presence of Hg^{2+} were acquired. As shown in Fig. 1C, the CD spectrum of the probe itself showed a random coil (curve a), whereas the CD spectrum of the probe incubated with 20 nM Hg^{2+} (curve b) presented a positive band centered at a wavelength of 280 nm together with a negative band at 250 nm. This result was in accordance with the CD spectrum of Hg^{2+}-aptamer-1 in the presence of 8 μM Hg^{2+},[39] indicating the C–Hg^{2+}-aptamer-1-AgNCs formed a hairpin structure in the presence of Hg^{2+}. In addition, the UV-Vis absorption spectra and fluorescence spectra of C–Hg^{2+}-aptamer-2-AgNCs alone and with 10 nM Hg^{2+} are shown in Fig. S2.† Both the absorption spectrum of C–Hg^{2+}-aptamer-2-Ag NCs alone (curve a) and that with 10 nM Hg^{2+} (curve b) showed a strong peak at 430 nm and a weak band at about 550 nm. Fig. S2B and C† show the fluorescence emission spectra of, respectively, C–Hg^{2+}-aptamer-2-AgNCs alone and with 10 nM Hg^{2+}, under various excitation wavelengths. Upon excitation at 570 nm, C–Hg^{2+}-aptamer-2-AgNCs alone and that with 10 nM Hg^{2+} each presented a maximum emission peak at a wavelength of 622 nm. In accordance with the results of C–Hg^{2+}-aptamer-1-AgNCs, the fluorescence intensity of the latter was 5.6 times stronger than that of the former (Fig. S2D†). The CD spectrum of C–Hg^{2+}-aptamer-2-AgNCs with 20 nM Hg^{2+} (Fig. S2E†) demonstrated that Hg^{2+}-aptamer-2 also formed the hairpin structure when Hg^{2+} was added.[39]

According to the above results, the enhancement of the fluorescence intensity of the C–Hg^{2+}-aptamer-1-AgNCs after incubating with 10 nM Hg^{2+} was greater than that of the C–Hg^{2+}-aptamer-2-AgNCs in the same condition. Thus, we further investigated the properties of the C–Hg^{2+}-aptamer-1-AgNCs probe alone and with Hg^{2+}. The fluorescence lifetimes at a wavelength of 620 nm of the C–Hg^{2+}-aptamer-1-Ag NCs incubated with and without the target Hg^{2+} were first measured (Fig. S3†). The fluorescence transients of C–Hg^{2+}-aptamer-1-Ag NCs presented the tri-exponential time constants as tabulated in Table S2.† The results illustrated that there were no obvious differences between the average fluorescence lifetimes of C–Hg^{2+}-Aptamer-1-AgNCs in the absence and presence of different concentrations of Hg^{2+}, further demonstrating a static interaction mechanism. Furthermore, the acquired TEM image of C–Hg^{2+}-aptamer-1-AgNCs in the presence of 10 nM Hg^{2+} illustrated the formation of uniformly dispersed and nearly spherical DNA–AgNCs with an average diameter of nearly 2 nm (Fig. 1D). XPS was performed to determine whether various elements were present and to determine the valence state of the Ag element in the C–Hg^{2+}-aptamer-1-AgNCs. As shown in Fig. 1E, the presence of B, C, N, O, P, Na and Ag was confirmed. The percentage of the AgNCs consisting of Ag was calculated from the peak areas of the elements to be 0.65%. As shown in the magnified view of the spectrum in its Ag 3d region (Fig. 1F), binding energy values at 368.2 eV for Ag $3d_{5/2}$ and 374.2 eV for Ag $3d_{3/2}$ were observed, confirming the presence of elemental Ag(0) in the C–Hg^{2+}-aptamer-1-AgNCs.[40]

3.2 Optimization of experimental conditions for Hg^{2+} determination

3.2.1 Optimization of pH. The fluorescence of AgNCs has been shown to be dependent on pH, and changing the pH would lead to obvious fluorescence quenching.[31] Fig. S4A† shows a plot of F/F_0 of C–Hg^{2+}-aptamer-1-AgNCs as a function of pH, where F_0 and F are the maximum emission intensities of the DNA–AgNCs without and with 10 nM Hg^{2+}, respectively. Here, F/F_0 of C–Hg^{2+}-aptamer-1-AgNCs increased as the pH was increased from 5 to 6.6 and then decreased as the pH was further increased from 6.6 to 9, indicating that the performance of this sensor was the best at pH 6.6. Similarly, the relative fluorescence intensity of C–Hg^{2+}-aptamer-2-AgNCs with 10 nM Hg^{2+} was maximum for a pH value of 6.3 (Fig. S4B†).

3.2.2 Optimization of detection time. As shown in Fig. S5A,† the fluorescence of the C–Hg^{2+}-aptamer-1-AgNCs incubated with 10 nM Hg^{2+} reached a maximum, and sustained it for nearly one hour, after the AgNCs were also incubated with $NaBH_4$ for 2.5 hours. However, for the C–Hg^{2+}-aptamer-2-AgNCs with 10 nM Hg^{2+}, the fluorescence increased to the maximum after one hour and then decreased rapidly to a minimum after 1.75 hours (Fig. S5B†). Test of the stability of the probe itself also gave a similar result (Fig. S6†). The

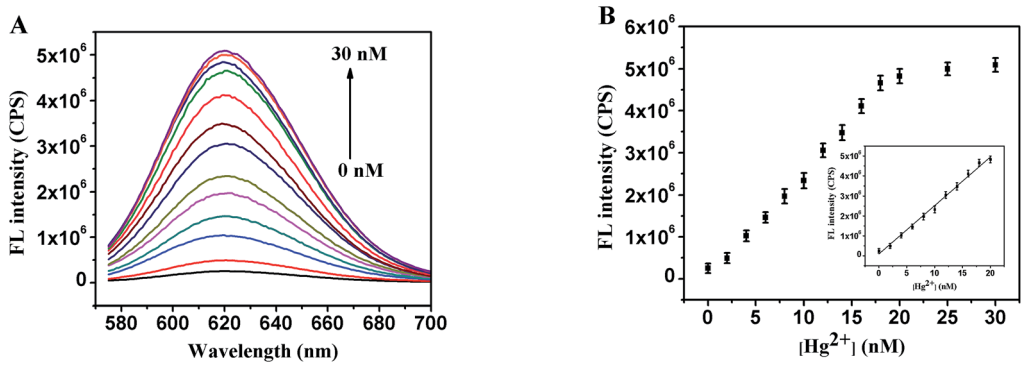

Fig. 2 (A) Fluorescence emission spectra (λ_{ex} = 560 nm) of C–Hg^{2+}-aptamer-1-AgNCs resulting from the addition of various concentrations of Hg^{2+}. (B) Fluorescence emission intensity at a wavelength of 620 nm as a function of Hg^{2+} concentration. The inset shows the linear range of the plot in the main figure; this linear region encompassed concentrations of 2–18 nM (R = 0.9985). Each error bar represents the standard deviation of three independent measurements.

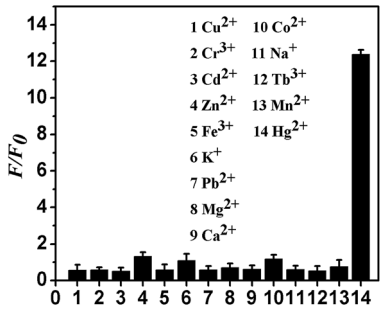

Fig. 3 Selectivity of C–Hg^{2+}-aptamer-1-AgNCs to different metal cations. Each bar shows the relative fluorescence emission intensity (F/F_0) of C–Hg^{2+}-aptamer-1-Ag NCs upon the addition of 10 nM Hg^{2+} and 100 nM of another ionic metal. F_0 and F represent the maximum emission intensities of the DNA–AgNCs, respectively, before and after addition of the ionic metal.

strongest fluorescence intensity of the C–Hg^{2+}-aptamer-1-AgNC probe was observed to be maintained for about 1.5 hours (Fig. S6A†), but the fluorescence intensity of the C–Hg^{2+}-aptamer-2-AgNC probe decreased rapidly after reaching the maximum value (Fig. S6B†). So C–Hg^{2+}-aptamer-1-AgNCs and C–Hg^{2+}-aptamer-2-AgNCs were used to perform the experiments described below after being prepared for 2.5 hours and 1 hour, respectively.

3.2.3 Detection of Hg^{2+}. To evaluate, under optimal conditions, the analytical performance of the method, including its detection limit and the linearity of its plots, the fluorescence of C–Hg^{2+}-aptamer-1-AgNCs was monitored upon adding various concentrations of Hg^{2+}. As shown in Fig. 2A, the fluorescence intensity of C–Hg^{2+}-aptamer-1-AgNCs continually increased as the concentration of Hg^{2+} was increased from 2 to 30 nM. A good linear relationship ($R = 0.9985$) was observed within the range 2 to 18 nM (Fig. 2B) with a detection limit (LOD) of 0.25 nM (S/N = 3) based on $3\sigma_0/k$, where σ_0 is the standard deviation of background and k is the slope of the calibration line. This detection limit is much lower than the maximum allowable level of inorganic Hg^{2+} in drinking water (10 nM) according to the U.S. Environmental Protection Agency (EPA) standard[41] and is also below the maximum permissible limit of mercury in drinking water (5 nM) permitted by the European Union.[15] For comparison, the detection limits and linear ranges for Hg^{2+} detection by other sensors are listed in Table S3.† The sensitivity of our method was much lower than those of the other methods.[14,31,42–46] These results demonstrated that the proposed sensor we developed for the quantitative analysis of Hg^{2+} provided a good linear plot of signal to Hg^{2+} concentration and a high sensitivity for Hg^{2+}. We also tested C–Hg^{2+}-aptamer-2-AgNCs for the detection of Hg^{2+}. As shown in Fig. S7A,† the change in the fluorescence of C–Hg-aptamer-2-AgNCs as a result of changes in the concentrations of added Hg^{2+} was in accordance with that of C–Hg^{2+}-aptamer-1-AgNCs. As shown in Fig. S7B,† C–Hg^{2+}-aptamer-1-AgNCs also yielded a good linear plot from 2 to 18 nM ($R = 0.9972$) with a detection limit (LOD) of 0.8 nM. Comparing the sensitivity and stability of the two kinds of DNA–AgNCs indicated the C–Hg^{2+}-aptamer-1-AgNC probe to be better, so we used it for the subsequent experiments.

3.2.4 Selectivity of C–Hg^{2+}-aptamer-1-Ag NCs for detecting Hg^{2+}. To investigate the specificity of C–Hg^{2+}-aptamer-1-Ag NC sensing system, other metal ions were also investigated using the above strategy. As shown in Fig. 3, only Hg^{2+} (10 nM) caused a significant increase in the relative fluorescence intensity (F/F_0), and even a high concentration of any of the other metal ions (100 nM), specifically including Cu^{2+}, Cr^{3+}, Cd^{2+}, Zn^{2+}, Fe^{3+}, K^+, Pb^{2+}, Mg^{2+}, Ca^{2+}, Co^{2+}, Na^+, Tb^{3+}, and Mn^{2+}, only caused a negligible increase in the fluorescence of C–Hg^{2+}-aptamer-1-AgNCs. We attributed this specificity for Hg^{2+} to the presence of the thymine (T)-rich sequence segment in the middle of the DNA portion of the C–Hg^{2+}-aptamer-1-AgNC probe, as Hg^{2+} can specifically bind to two thymine (T) residues of DNA to form a T–Hg^{2+}–T complex.[35] The results clearly demonstrated this sensor to be highly selective for Hg^{2+}, and the proposed approach could thus be used to specifically detect Hg^{2+} in biological and environmental samples.

3.2.5 Analytical applications. To evaluate the practical application of the proposed sensor, tap water and lake water (from Shanxi University) were monitored by using this method. The water samples were filtered three times through qualitative filter paper and centrifuged, and the supernatants were used for the quantitative analysis. Hg^{2+} was not detected in these real samples because the concentration of Hg^{2+} was much lower than the detection limit of the C–Hg^{2+}-aptamer-1-AgNCs sensing system. So these samples were spiked with different standard Hg^{2+} solutions, and the average values of the results

Table 1 Recoveries of Hg^{2+} in water samples detected using the proposed Hg^{2+} assay ($N = 3$)

		C–Hg^{2+}-aptamer-1-AgNCs	C–Hg^{2+}-aptamer-1-AgNCs
Samples	Spiked (nM)	Measured (nM), mean[a] ± SD[b]	Recovery (%)
Lake water 1	5	5.315 ± 0.13	106.3
Lake water 2	10	10.06 ± 0.06	100.6
Lake water 3	15	15.08 ± 0.12	100.5
Tap water 1	5	5.102 ± 0.07	102.0
Tap water 2	10	10.13 ± 0.21	101.3
Tap water 3	15	14.89 ± 0.32	99.27

[a] The mean of three determinations. [b] SD = standard deviation.

for three replicate determinations are listed in Table 1. The recoveries varied from 99.27% to 106.3%, and standard deviations were all less than 0.32. These results revealed the developed method to be reliable for assaying Hg^{2+} in environmental water samples.

4 Conclusions

In summary, a novel strategy for the detecting Hg^{2+} has been developed using C–Hg^{2+}-aptamer-DNA-stabilized AgNCs as a turn-on fluorescent probe based on an Hg^{2+}-induced conformational transition of Hg^{2+}-aptamer-DNA. This sensor presented high sensitivity and selectivity with an LOD of 0.25 nM that met the requirements of industrial and environmental monitoring applications. This novel sensing assay was a low-cost, turn-on, and sensitive assay and could be easily performed by carrying out simple mixing. In addition, it was also successfully applied to practical situation, specifically the detection of Hg^{2+} in real water samples. So the proposed sensing system is considered to have the potential to be a useful tool for detection of Hg^{2+} in environmental water.

Conflicts of interest

There are no conflicts to declare.

Acknowledgements

This work was supported by the National Natural Science Foundation of China (21171108) and Shanxi Provincial Fund for Natural Sciences (201601D011026).

Notes and references

1 M. Zaib, M. Athar, A. Saeed and U. Farooq, *Biosens. Bioelectron.*, 2015, **74**, 895–908.
2 Z. Li, Y. Ni and S. Kokot, *Biosens. Bioelectron.*, 2015, **74**, 91–97.
3 E. M. Nolan and S. J. Lippard, *Chem. Rev.*, 2008, **108**, 3443–3480.
4 D. Han, Y.-R. Kim, J.-W. Oh, T. H. Kim, R. K. Mahajan, J. S. Kim and H. Kim, *Analyst*, 2009, **134**, 1857–1862.
5 C. Rusinek, A. Bange, I. Papautsky, W. Heineman, J. Chen, S. Zhou and J. Wen, *Anal. Chem.*, 2014, **86**, 3108–3114.
6 K. Kristian, S. Friedbauer, D. Kabashi, K. Ferencz, J. Barajas and K. Brien, *J. Chem. Educ.*, 2015, **92**, 698–702.
7 F. Han, W. Patterson, Y. Xia, B. Sridhar and Y. Su, *Water, Air, Soil Pollut.*, 2006, **170**, 161–171.
8 H. Cheng and Y. Qian, *Sens. Actuators, B*, 2015, **219**, 57–64.
9 R. Huang, X. Li, Q. Gai, G. Liu and Z. Wei, *Biosens. Bioelectron.*, 2015, **71**, 194–199.
10 B. M. W. Fong, T. S. Siu, J. S. K. Lee and S. Tam, *J. Anal. Toxicol.*, 2007, **37**, 281–287.
11 D. Malinovsky, R. E. Sturgeon and L. Yang, *Anal. Chem.*, 2008, **80**, 2548–2555.
12 L. Dong, X. Yan, Y. Li, Y. Jiang, S. Wang and D. Jiang, *J. Chromatogr., A*, 2004, **1036**, 119–125.
13 J. L. Gomez-Ariza, F. Lorenzo and T. Garcia-Barrera, *Anal. Bioanal. Chem.*, 2005, **382**, 485–492.
14 L. Deng, Z. Zhou, J. Li, T. Li and S. Dong, *Chem. Commun.*, 2011, **47**, 11065–11067.
15 B. Adhikari and A. Banerjee, *Chem. Mater.*, 2010, **22**, 4364–4371.
16 C. Guo and J. Irudayaraj, *Anal. Chem.*, 2011, **83**, 2883–2889.
17 H. Wei, Z. Wang, L. Yang, S. Tian, C. Hou and Y. Lu, *Analyst*, 2010, **135**, 1406–1410.
18 S. Choi, R. M. Dickson and J. Yu, *Chem. Soc. Rev.*, 2012, **41**, 1867–1891.
19 L. Shang, S. Dong and G. U. Nienhaus, *Nano Today*, 2011, **6**, 401–418.
20 N. Liu, S. Mukherjee, K. Bao, Y. Li, L. Brown, P. Nordlander and N. Halas, *ACS Nano*, 2012, **6**, 5482–5488.
21 J. Petty, J. Zhang, N. Hud and R. Dickson, *J. Am. Chem. Soc.*, 2004, **126**, 5207–5212.
22 T. Udayabhaskararao and T. Pradeep, *J. Phys. Chem. Lett.*, 2013, **4**, 1553–1564.
23 N. Zhang, Y. Si, Z. Sun, L. Chen, R. Li, Y. Qiao and H. Wang, *Anal. Chem.*, 2014, **86**, 11714–11721.
24 A. Fihey, F. Maurel and A. Perrier, *J. Phys. Chem. C*, 2014, **118**, 4444–4453.
25 Y. Antoku, Fluorescent poly-cytosine-encapsulated silver nanoclusters, PhD thesis, Georgia Institute of Technology, 2007.
26 J. L. MacLean, K. Morishita and J. Liu, *Biosens. Bioelectron.*, 2013, **48**, 82–86.
27 C. I. Richards, S. Choi, J. Hsiang, Y. Antoku, T. Vosch, A. Bongiorno, Y. Tzeng and R. M. Dickson, *J. Am. Chem. Soc.*, 2008, **130**, 5038–5039.
28 E. G. Gwinn, P. O'Neill, A. J. Guerrero, D. Bouwmeester and D. K. Fygenson, *Adv. Mater.*, 2008, **20**, 279–283.
29 B. Han and E. Wang, *Anal. Bioanal. Chem.*, 2012, **402**, 129–138.
30 A. Ono, S. Cao, H. Togashi, M. Toshiro, T. Fujimoto, T. Machinami, S. Oda, Y. Miyake, I. Okamoto and Y. Tanaka, *Chem. Commun.*, 2008, **39**, 4825–4827.
31 W. Guo, J. Yuan and E. Wang, *Chem. Commun.*, 2009, **45**, 3395–3397.
32 C. Li and C. Wei, *Sens. Actuators, B*, 2017, **242**, 563–568.
33 Y. Tao, Y. Lin, Z. Huang, J. Ren and X. Qu, *Talanta*, 2012, **88**, 290–294.
34 B. Yin, J. Ma, H. Le, S. Wang, Z. Xu and B. Ye, *Chem. Commun.*, 2014, **50**, 15991–15994.
35 Y. Miyake, H. Togashi, M. Tashiro, H. Yamaguchi, S. Oda, M. Kudo, Y. Tanaka, Y. Kondo, R. Sawa, T. Fujimoto, T. Machinami and A. Ono, *J. Am. Chem. Soc.*, 2006, **128**, 2172–2173.
36 J. Xu and C. Wei, *Biosens. Bioelectron.*, 2017, **87**, 422–427.
37 X. Liu, R. Hu, Z. Gao and N. Shao, *Langmuir*, 2015, **31**, 5859–5867.
38 E. Shaviv, O. Schubert, M. Alves-Santos, G. Goldoni, R. D. Felice, F. Vallée, N. Fatti, U. Banin and C. Sönnichsen, *ACS Nano*, 2011, **5**, 4712–4719.
39 J. Xu, Z. Song, Y. Fang, J. Mei, L. Jia, A. J. Qin, J. Z. Sun, J. Ji and B. Z. Tang, *Analyst*, 2010, **135**, 3002–3007.

40 Z. K. Wu, *Angew. Chem., Int. Ed.*, 2012, **51**, 2934–2938.
41 U. S. EPA, *EPA-452/R-05-003*, U. S. Government Printing Office, Washington, DC, 2005.
42 W. Chansuvarn and A. Imyim, *Microchim. Acta*, 2012, **176**, 57–64.
43 G. Liang, L. Wang, H. Zhang, Z. Han and X. Wu, *Microchim. Acta*, 2012, **179**, 345–350.
44 R. Z. Wang, D. L. Zhou, H. Huang, M. Zhang, J. J. Feng and A. J. Wang, *Microchim. Acta*, 2013, **180**, 1287–1293.
45 C. Chiang, C. Huang, C. Liu and H. Chang, *Anal. Chem.*, 2008, **80**, 3716–3721.
46 H. Park, S. Hwang and K. Kim, *Electrochem. Commun.*, 2012, **24**, 100–103.